Protonated Ethane. A Theoretical Investigation of $C_2H_7^+$ Structures and Energies

José Walkimar de M. Carneiro,[†,‡] Paul von R. Schleyer,*[,‡] Martin Saunders,[§] Richard Remington,[⊥] Henry F. Schaefer III,[⊥] Arvi Rauk,[∥] and Theodore S. Sorensen[∥]

Contribution from the Computer Chemistry Center, Institut für Organische Chemie der Friedrich-Alexander Universität Erlangen-Nürnberg, Henkestrasse 42, D-91054 Erlangen, Germany, Department of Chemistry, Yale University, New Haven, Connecticut 06520, Center for Computational Quantum Chemistry, University of Georgia, Athens, Georgia 30602, and Department of Chemistry, University of Calgary, Calgary, Alberta, Canada T2N 1N4

Received March 24, 1993. Revised Manuscript Received October 28, 1993[⊗]

Abstract: The $C_2H_7^+$ potential energy surface was characterized by high-level *ab initio* calculations. The effects of electron correlation on geometries and relative energies are substantial. At MP4(SDTQ)/6-311G**//MP2(full)/6-31G**, the global minimum is the C–C protonated structure **1**, 4.4 kcal/mol (corrected to 298 K) more stable than the C–H protonated form **3**. The proton affinity of ethane to give **1** (142.5 kcal/mol) is 12.5 kcal/mol greater than that of methane (130 kcal/mol). Methane adds to the methyl cation, leading to **1** without activation energy. Barriers for intramolecular hydrogen interchange are lower than the dissociation energy into the ethyl cation and hydrogen, consistent with the experimental observation that deuterium scrambling is faster than dissociation. $C_2H_7^+$ loses H_2 by 1,1-elimination in an endothermic (10.6 kcal/mol) process. Three frequencies deduced experimentally for $C_2H_7^+$ correspond to those computed for **1**, but neither **2**, the H_2-rotated C–H protonated form, nor **3** can explain the other set of experimental spectral data. Complexes between H_2 and bridged $C_2H_5^+$ were located, but they are too weakly bonded to be detected experimentally.

Protonated alkanes are important intermediates in saturated hydrocarbon transformations.[1] These nonclassical carbonium ions usually are characterized by three-center, two-electron bonded structures having pentacoordinated carbon atoms and bridging hydrogens.[1-3] The simplest alkonium ion, CH_5^+, was first reported by Tal'roze and Lyubimova.[4] Higher homologues ($C_nH_{2n+3}^+$) also were detected later in high-pressure mass spectrometry experiments.[5] These carbonium ions are formed in the gas phase by ion–molecule reactions involving primary ions and neutral hydrocarbons or through simple proton-transfer reactions between the methonium ion and higher alkanes.

As part of an extensive investigation of electrophilic reactions of single bonds, Olah et al. examined the behavior of simple alkonium ions.[1a,b,6] While these species are not directly observable in superacid solution, methane and ethane undergo hydrogen exchange and polycondensation to produce tertiary alkyl cations. This alkane condensation is assumed to start with reversible methane protonation leading to the methonium ion, CH_5^+. This species is believed to lose a hydrogen molecule to form the highly reactive (but not directly observable) methyl cation. CH_3^+ reacts with excess methane to form the ethonium ion, $C_2H_7^+$, which in turn decomposes into H_2 and the ethyl cation (eq 1). The process of building up higher carbocations continues with the reaction of $C_2H_5^+$ with methane.

$$CH_3^+ + CH_4 \rightarrow C_2H_7^+ \rightarrow C_2H_5^+ + H_2 \qquad (1)$$

Protonated ethane, $C_2H_7^+$, is the key intermediate in this mechanism. Olah and co-workers proposed that protolytic cleavage reactions and hydrogen–deuterium exchange as well as polycondensation of alkanes in superacid systems take place through protolysis of C–C or C–H bonds. These single bonds act as σ-electron donors; protonation leads to transition states or intermediates characterized by three-center bonded pentacoordinated carbonium ions.[6g] Olah and co-workers were the first to note that various protonation sites are possible for ethane and the higher alkanes.[6b] Ethane itself prefers C–C over C–H bond protonation.[6c] An essentially symmetrical H-bridged structure was suggested to be the preferred form of the ethonium ion, $C_2H_7^+$.

As the loss of H_2 from CH_5^+ is quite endothermic, an alternative mechanism which circumvents the formation of CH_3^+ in a discrete step is conceivable. The H_2 loss from CH_5^+ and the reaction with CH_4 might be concerted (eq 2). Indeed, not only $C_2H_9^+$ but also

$$CH_5^+ + CH_4 \rightarrow C_2H_9^+ \rightarrow C_2H_7^+ + H_2 \rightarrow C_2H_5^+ + 2H_2 \qquad (2)$$

[†] Permanent address: UFF-Instituto de Química, Department of Inorganic Chemistry, Outeiro de Sao Joao Batista-3° Andar, 24020-Niterof-RJ, Brazil.
[‡] Universität Erlangen-Nürnberg.
[§] Yale University.
[⊥] University of Georgia.
[∥] University of Calgary.
[⊗] Abstract published in *Advance ACS Abstracts,* February 1, 1994.

(1) (a) Olah, G. A.; Prakash, G. K. S.; Williams, R. E.; Field, L. D.; Wade, K. *Hypercarbon Chemistry*; Wiley-Interscience: New York, 1987; p 148f. (b) Olah, G. A.; Prakash, G. K. S.; Sommer, J. *Superacids*; Wiley-Interscience: New York, 1985; p 125f. (c) Vogel, P. *Carbocation Chemistry*; Elsevier: Amsterdam, 1985; pp 63, 103, 167.

(2) For a discussion of three-center bonded systems see ref 1a, p 13f, ref 1b, and ref 3.

(3) Olah, G. *J. Am. Chem. Soc.* **1972**, *94*, 808–820.

(4) Tal'roze, V. L.; Lyubimova, A. K. *Dokl. Akad. Nauk SSSR* **1952**, *86*, 909–912; *Chem. Abstr.* **1953**, *47*, 2590g.

(5) (a) Wexler, S.; Jesse, N. *J. Am. Chem. Soc.* **1962**, *84*, 3425–3432. (b) Field, F. H.; Franklin, J. L.; Munson, M. S. B. *J. Am. Chem. Soc.* **1963**, *85*, 3575–3583. (c) Field, F. H.; Munson, M. S. B. *J. Am. Chem. Soc.* **1965**, *87*, 3289–3294. (d) Munson, M. S. B.; Field, F. H. *J. Am. Chem. Soc.* **1965**, *87*, 3294–3299 and references cited therein. (e) Aquilanti, V.; Volpi, G. G. *J. Chem. Phys.* **1966**, *44*, 2307–2313. (f) For a summary, see: Field, F. H. *Acc. Chem. Res.* **1968**, *1*, 42–49.

(6) (a) Olah, G. A.; Lukas, J. *J. Am. Chem. Soc.* **1967**, *89*, 2227–2228. (b) Olah, G. A.; Klopman, G.; Schlosberg, R. H. *J. Am. Chem. Soc.* **1969**, *91*, 3261–3268. (c) Olah, G. A.; Halpern, Y.; Shen, J.; Mo, Y. K. *J. Am. Chem. Soc.* **1971**, *93*, 1251–1256. (d) Olah, G. A.; Olah, J. A. *J. Am. Chem. Soc.* **1971**, *93*, 1256–1259. (e) Olah, G. A.; Mo, Y. K.; Olah, J. A. *J. Am. Chem. Soc.* **1973**, *95*, 4939–4951. (f) Olah, G. A.; DeMember, J. R.; Shen, J. *J. Am. Chem. Soc.* **1973**, *95*, 4952–4956. (g) Olah, G. A.; Halpern, Y.; Shen, J.; Mo, Y. K. *J. Am. Chem. Soc.* **1973**, *95*, 4960–4970.

0002-7863/94/1516-3483$04.50/0

higher $CH_5^+(CH_4)_n$ complexes are observed in the gas phase.[7b,8] Although several authors have studied proton–deuterium exchange and randomization in the $C_2H_7^+$ system,[9] Saunders, Cross, et al.[10] were the first to carry out experiments designed to gain more specific structural information. Deuterium-labeled methane and methyl cations were employed to investigate the scrambling and dissociation mechanisms. After decomposition, the end products are the ethyl cation and a hydrogen molecule (eq 1). On the assumptions that the extra proton is associated with one but not both of the carbon atoms (i.e., H_3C–CH_4^+) and that the decomposition of $C_2H_7^+$ always takes place from the pentacoordinated carbon atom by 1,1-elimination, a kinetic model was proposed to explain the H-scrambling observed. This occurs through an $C_2H_7^+$ intermediate which is short-lived but sufficiently well-defined to permit deuterium scrambling before decomposition occurs.[10]

Starting in 1975, Kebarle et al. reported a quantitative investigation of several protonated alkanes using high-pressure ion source mass spectrometry.[7,8] For example, French and Kebarle's direct measurement of the decomposition of $C_2H_7^+$ into $C_2H_5^+$ and H_2 gave $E = 10.5 \pm 2.0$ kcal/mol.[7c] By studying the rates and equilibria for addition of H_2 to $C_2H_5^+$, Hiraoka and Kebarle observed that two different $C_2H_7^+$ isomers were produced, depending on temperature.[8] At very low temperatures (−130 °C to −160 °C), H_2 added to $C_2H_5^+$ to form a $C_2H_7^+$(a) species in an exothermic third-body-dependent reaction without activation energy. At temperatures above −130 °C, the $C_2H_7^+$(a) species started to rearrange, and between −100 °C and +40 °C, a new and more stable $C_2H_7^+$(b) species was formed. At temperatures between 40 °C and 200 °C, the $C_2H_7^+$(b) ion decomposed back into $C_2H_5^+ + H_2$. The $C_2H_7^+$(a) isomer was identified as a C–H protonated ethane, while the more stable $C_2H_7^+$(b) was considered to be a C–C protonated form.

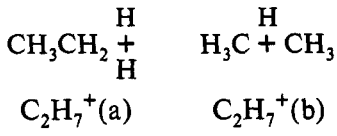

The activation energy for conversion of $C_2H_5^+ + H_2$ into $C_2H_7^+$(b) was estimated to be 1.2 kcal/mol via kinetic measurements in the −100 °C to +40 °C range. Measurements of the temperature dependence of the equilibrium $C_2H_5^+ + H_2 \rightleftharpoons C_2H_7^+$ gave $\Delta H_a = -4.0$ kcal/mol and $\Delta H_b = -11.8$ kcal/mol for the low- and high-temperature species, respectively. These data imply that the activation energy for loss of H_2 from $C_2H_7^+$(b) should be 1.2 + 11.8, 1.8, or 13.0, kcal/mol. This was larger than the directly-measured 10.5 kcal/mol reported earlier,[7c] but both values were considered to be in agreement, considering the "expected error limit". The energy barrier for the isomerization of $C_2H_7^+$(a) into $C_2H_7^+$(b) was deduced to be 5.2 kcal/mol.[8] Kebarle's experimental results are summarized in Figure 1. This figure is also based on thermochemical data for the other species, CH_4, CH_3^+, and $C_2H_5^+$.

Saunders and Cross's findings require that deuterium scrambling, starting with labeled CH_3^+ and CH_4, occurs before dissociation into H_2 and $C_2H_5^+$ takes place. This implies that the barrier to scrambling is lower than the dissociation energy.[10] Kebarle's results indicate the C–H protonated form ($C_2H_7^+$(a)) to be formed first from $C_2H_5^+$ and H_2;[8] $C_2H_7^+$(a) is also the species from which loss of H_2 is believed to occur. Scrambling may occur prior to conversion into $C_2H_7^+$(b), but this process, according to Kebarle's newer data, requires a higher activation energy than decomposition into $C_2H_5^+$ and H_2. In the crossed-beam experiment, the reactant species have excess energy when they combine and cannot relax unless collision with a third body takes place. Hence, more than sufficient energy is available for rearrangements. This can be followed by a further step leading, e.g., back to the original chemical structure with rearranged isotopes.

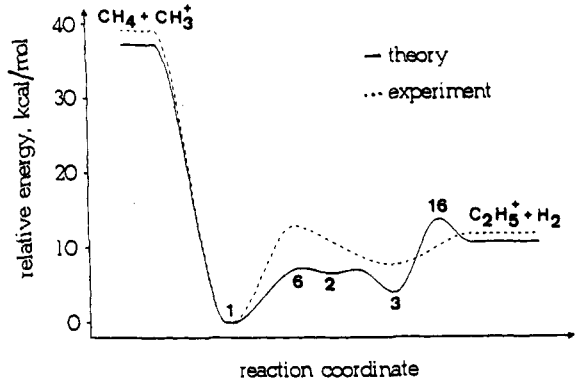

Figure 1. Potential energy diagram for reaction 1. Dashed curve is based on data from ref 8. The full curve is based on data from this work.

More recently, Lee et al. were able to deduce the infrared spectrum of the $C_2H_7^+$ ion.[11] They observed two sets of spectral features which were attributed to two different kinds of $C_2H_7^+$ structures. By analyzing the dependence of band intensities on the backing pressure and on the mixing ratio of hydrogen to ethane, these authors assigned the experimentally observed frequencies to the vibrational modes in the C–C and C–H protonated structures. In particular, they assigned a frequency at 3964 cm^{-1} to the H–H stretching vibration in a loose $C_2H_5^+ \cdot H_2$ complex.[11] This frequency was compared with those of other H_2 complexes but did *not* receive support from the (privately communicated)[11] *ab initio* computed spectra of Dupuis.

As all the experiments described above give only general information about structure, a complementary theoretical examination is indispensable. This is particularly so for such a system whose unusual characteristics may determine its behavior. The structure of CH_5^+ has been investigated extensively by theoretical methods,[12–15] but the potential energy surface of protonated ethane, $C_2H_7^+$, is significantly more complicated and has not been elucidated fully.[16] Earlier theoretical studies on $C_2H_7^+$ all agreed that the C–C protonated species is more stable

(7) (a) Hiraoka, K.; Kebarle, P. *J. Chem. Phys.* **1975**, *63*, 394–397. (b) Hiraoka, K.; Kebarle, P. *J. Am. Chem. Soc.* **1975**, *97*, 4179–4183. (c) French, M.; Kebarle, P. *Can. J. Chem.* **1975**, *53*, 2268–2274. (d) Hiraoka, K.; Kebarle, P. *Can. J. Chem.* **1975**, *53*, 970–972.

(8) (a) Hiraoka, K.; Kebarle, P. *J. Am. Chem. Soc.* **1976**, *98*, 6119–6125. (b) Hiraoka, K.; Kebarle, P. *Adv. Mass Spectrom.* **1978**, *7b*, 1408–1418.

(9) (a) Huntress, W. T., Jr. *J. Chem. Phys.* **1972**, *56*, 5111–5120. (b) Herman, Z.; Hierl, P.; Lee, A.; Wolfgang, R. *J. Chem. Phys.* **1969**, *51*, 454–455. (c) Ding, A.; Henglein, A.; Lacmann, K. *Z. Naturforsch.* **1968**, *23A*, 780–781. (d) Abramson, F. P.; Futrell, J. H. *J. Chem. Phys.* **1966**, *45*, 1925–1931. (e) Bohme, D. K.; Fennelly, P.; Hemsworth, R. S.; Schiff, H. I. *J. Am. Chem. Soc.* **1973**, *95*, 7512–7513.

(10) Weiner, J.; Smith, G. P. K.; Saunders, M.; Cross, R. J., Jr. *J. Am. Chem. Soc.* **1973**, *95*, 4115–4120. Cf. Heck, A. J. R.; deKoning, L. J.; Nibbering, N. M. M. *Int. J. Mass. Spectrom. Ion Processes* **1992**, *117*, 145.

(11) Yeh, L. I.; Price, J. M.; Lee, Y. T. *J. Am. Chem. Soc.* **1989**, *111*, 5597–5604.

(12) (a) Lathan, W. A.; Hehre, W. J.; Pople, J. A. *J. Am. Chem. Soc.* **1971**, *93*, 808–815. (b) Lathan, W. A.; Lehre, W. J.; Curtiss, L. A.; Pople, J. A. *J. Am. Chem. Soc.* **1971**, *93*, 6377–6387. (c) Hariharan, P. C.; Lathan, W. A.; Pople, J. A. *Chem. Phys. Lett.* **1972**, *14*, 385–388. (d) Schleyer, P. v. R.; Apeloig, Y.; Arad, D.; Luke, B. T.; Pople, J. A. *Chem. Phys. Lett.* **1983**, *95*, 477.

(13) (a) Raghavachari, K.; Whiteside, R. A.; Pople, J. A.; Schleyer, P. v. R. *J. Am. Chem. Soc.* **1981**, *103*, 5649–5657. (b) Schleyer, P. v. R.; Carneiro, J. W. de M. *J. Comput. Chem.* **1992**, *13*, 997–1003. (c) Schreiner, P. R.; Kim, S.-J.; Schleyer, P. v. R.; Schaefer, H. F., III. *J. Chem. Phys.* **1993**, *99*, 3716–3720.

(14) (a) Klopper, W.; Kutzelnigg, W. *J. Phys. Chem.* **1990**, *94*, 5625–5630. (b) Dyczmons, V.; Staemmler, V.; Kutzelnigg, W. *Chem. Phys. Lett.* **1970**, *5*, 361–366. (c) Kollmar, H.; Smith, H. O. *Chem. Phys. Lett.* **1970**, *5*, 7–9. (d) Gamba, A.; Morosi, G.; Simonetta, M. *Chem. Phys. Lett.* **1969**, *3*, 20–21.

(15) (a) Bischof, P. K.; Dewar, M. J. S. *J. Am. Chem. Soc.* **1975**, *97*, 2278–2280. (b) Hirao, K.; Yamabe, S. *Chem. Phys.* **1984**, *89*, 237–244.

(16) (a) Random, L.; Poppinger, D.; Haddon, R. C. In *Carbonium Ions*; Olah, G. A., Schleyer, P. v. R., Eds.; Wiley-Interscience: New York, 1976; Vol. 5, Chapter 38. (b) Hehre, W. J. In *Applications of Electronic Structure Theory*; Schaefer, H. F., III, Ed.; Plenum: New York, 1977; Chapter 7.

Table 1. Absolute Energies (-au) of $C_2H_7^+$ Isomers and Other Species Discussed in This Work

species	HF/6-31G*// HF/6-31G*	MP2(full)/6-31G*// MP2(full)/6-31G*	MP2(full)/6-31G**// MP2(full)/6-31G**	-/6-311G**//MP2(full)/6-31G**		
				MP2	MP3	MP4(sdtq)
1	79.455 24	79.726 34	79.784 34	79.800 56	79.833 72	79.847 57
1a	79.455 11	79.725 88	79.783 86	79.800 03	79.833 31	79.847 17
2	79.439 18	79.714 36	79.774 66	79.791 57	79.822 74	79.836 17
3	79.436 27	79.715 22	79.775 86	79.793 28	79.824 71	79.837 86
3a		79.715 22	79.775 86	79.793 26	79.824 67	79.837 82
4	79.427 22	79.712 18	79.773 98	79.791 31	79.822 01	79.835 16
5	79.432 37	79.711 99	79.772 65	79.789 92	79.821 29	79.834 40
6	79.428 38	79.712 83	79.772 87	79.789 94	79.820 37	79.834 02
7	79.452 87	79.717 11	79.774 39	79.789 44	79.824 20	79.838 92
16			79.752 55	79.769 64	79.821 29	79.818 09
C_2H_6	79.228 76	79.503 97	79.553 71	79.570 74	79.601 03	79.614 24
$C_2H_5^+$ (**8**)	78.309 94	78.561 45	78.601 18	78.613 27	78.640 27	78.653 21
$C_2H_5^+$ (**9**)	78.310 21	78.551 24	78.589 07	78.600 58	78.629 10	78.641 88
CH_5^+	40.388 50	40.536 33	40.580 28	40.590 11	40.609 89	40.616 56
CH_4	40.195 17	40.337 04	40.369 86	40.379 14	40.398 18	40.404 84
CH_3^+	39.230 64	39.329 44	39.351 20	39.356 10	39.374 80	39.379 56
H_2	1.126 83	1.144 14	1.157 66	1.160 26	1.166 21	1.168 10

Table 2. Relative Energies (kcal/mol) of $C_2H_7^+$ Isomers

species	HF/6-31G*// HF/6-31G*	MP2(full)/6-31G*// MP2(full)/6-31G*	MP2(full)/6-31G**// MP2(full)/6-31G**	-/6-311G**//MP2(full)/6-31G**			final[a]	exptl[b]
				MP2	MP3	MP4(sdtq)		
1	0.00	0.00	0.00	0.00	0.00	0.00	0.33	
1a	0.08	0.29	0.30	0.33	0.26	0.25	0.00	0.0
2	10.08	7.52	6.08	5.64	6.89	7.15	6.56	
3	11.91	6.98	5.32	4.57	5.65	6.09	4.43	7.8
3a		6.98	5.32	4.58	5.68	6.12	5.05	
4	17.59	8.89	6.50	5.81	7.35	7.79	5.77	
5	14.39	9.00	7.34	6.68	7.80	8.26	6.53	
6	16.86	8.48	7.20	6.67	8.38	8.50	7.16	13.0
7	1.49	5.79	6.24	6.98	5.97	5.43	3.15	
16			19.95	19.40	18.80	18.50	13.57	
$CH_4 + CH_3^+$	18.47	37.57	39.72	41.00	38.12	39.65	37.22	36
$H_2 + C_2H_5^+$	11.59	13.07	16.00	16.96	17.10	16.48	10.65	11.8
$C_2H_6 + H^+$	142.11	139.53	144.71	144.21	146.01	146.41	142.50	139.6

[a] Final is MP4(sdtq)/6-311G**//MP2(full)/6-31G** corrected to 298 K including zero-point vibrational energy plus vibrational, rotational, translational, and expansion work (ΔpV) contributions to H_{298}. Scaled vibrational frequencies (by 0.93) were used, and RT/2 was assigned to each rotational and translational degree of freedom. [b] Values deduced or employed in ref 8.

than the C–H protonated form[13a,15-18] but were inconclusive due to the technical limitations of the day. The theoretical levels employed for locating and characterizing the stationary points were inadequate, and some of the results are actually misleading. Hence, a systematic reexamination of this system is opportune. We employ *ab initio* molecular orbital theory at correlated levels to investigate geometries, energies, and vibrational frequencies of various $C_2H_7^+$ structures as well as the possible mechanisms for H-scrambling and for decomposition into $C_2H_5^+ + H_2$ and into $CH_3^+ + CH_4$. We analyze the potential energy surface in greater detail than has been done previously and discuss the effects of basis sets and correlation on structure and relative energies. The computed vibrational frequencies are compared with Lee's experimental results.[11]

Computational Methods

Optimizations and single-point calculations were carried out with the GAUSSIAN 90[19] package of molecular orbital programs (and earlier versions) at Erlangen and at Calgary. Vibrational frequencies at MP2-(full)/6-31G** were calculated with the CADPAC program.[20] Some geometries at HF/6-31G* and at MP2(full)/6-31G* already were available.[21,22] All our additional structures were fully optimized at both these levels; the only constraints employed maintained the symmetries specified. Since the ions studied here have delocalized σ-electron systems involving hydrogens, the use of basis sets with polarization functions on all atoms is desirable.[22] Hence, all geometries were reoptimized at MP2-(full)/6-31G**. The 6-31G** basis set also includes p-functions on all hydrogens; electron correlation effects are estimated at the full MP2 level. To refine the final relative energies, the MP2(full)/6-31G** geometries were further subjected to single-point MP4(SDTQ)/6-311G** calculations, i.e., with a triply split valence basis set and the Møller–Plesset (MP) perturbation treatment to complete (SDTQ) fourth order.[22] These single-point calculations employed the frozen core approximation. The total and the relative energies are given in Tables 1 and 2, respectively.

The nature of each stationary point was characterized by vibrational analysis. The geometries of some structures changed significantly on going from the Hartree–Fock to the correlated optimization level. Hence, besides the HF/6-31G* vibrational analysis, we have computed the MP2-(full)/6-31G** geometries as well. Zero-point energies, derived from the MP2(full)/6-31G** frequency calculations, are scaled (by 0.93)[23] and used to correct the relative energies. To assess enthalpy changes on going from 0 K to 298 K, $H - H_0$ was calculated at 298 K.[24] These values and zero-point energies are given in Table 3. Also given in Table 3 are the absolute entropies at 298 K. Our final relative energies are at MP4-(SDTQ)/6-311G**//MP2(full)/6-31G** corrected to 298 K. Unless otherwise specified, these are the values discussed in the text. The structures we considered are shown in Figures 2 and 3.

(17) Köhler, H.-J.; Lischka, H. *Chem. Phys. Lett.* **1978**, *58*, 175–179.
(18) Poirier, R. A.; Constantin, E.; Abbé, J. C.; Peterson, M. R.; Csizmadia, I. G. *J. Mol. Struct. (THEOCHEM)* **1982**, *88*, 343–355.
(19) Frisch, M. J.; Head-Gordon, M.; Trucks, G. W.; Foresman, J. B.; Schlegel, H. B.; Raghavachari, K.; Robb, M. A.; Binkley, J. S.; Gonzales, C.; DeFrees, D. J.; Fox, D. J.; Whiteside, R. A.; Seeger, R.; Melius, C. F.; Baker, J.; Martin, R. L.; Kahn, L. R.; Stewart, J. J. P.; Topiol, S.; Pople, J. A. *Gaussian 90*; Gaussian Inc.: Pittsburgh, PA, 1990.
(20) Amos, R. D.; Rice, J. E. *CADPAC: The Cambridge Analytic Derivatives Package*, Issue 4.0; Cambridge: U.K., 1987.
(21) *The Carnegie-Mellon Quantum Chemistry Archive*, 3rd ed.; Whiteside, R. A., Frisch, M. J., Pople, J. A., Eds.; Department of Chemistry, Carnegie-Mellon University, Pittsburgh, PA, 1983.
(22) For description of the basis set used in this work and Møller–Plesset perturbation theory, see: Hehre, W. J.; Radom, L.; Schleyer, P. v. R.; Pople, J. A. *Ab Initio Molecular Orbital Theory*; Wiley-Interscience: New York, 1986.
(23) Hout, R. F., Jr.; Levi, B. A.; Hehre, W. J. *J. Comput. Chem.* **1982**, *3*, 234–250.
(24) Enthalpy changes and absolute entropies were calculated with a program written by E. Kaufmann, based on the THERMO subroutine of MOPAC. We thank E. Kaufmann for furnishing us with the program.

Table 3. Zero-Point Energies, Enthalpy Change, and Absolute Entropies of $C_2H_7^+$ Isomers[a]

species	ZPE (kcal/mol)	$H_{298} - H_0$ (kcal/mol)[b]	S (eu)[b]
1	50.45 (0)[c]	3.35	60.77
1a	50.23 (1)	2.99	60.03
2	49.64 (0)	3.24	61.04
3	48.90 (1)	2.91	59.19
3a	48.98 (0)	3.42	63.44
4	48.46 (1)	2.99	59.61
5	48.77 (1)	2.97	59.67
6	49.09 (1)	3.04	59.99
7	48.09 (2)	3.10	58.79
16	44.84 (1)	3.70	64.51
C_2H_6	45.28 (0)	2.80	55.98
$C_2H_5^+$ (**8**)	36.87 (0)	2.57	54.61
CH_5^+	31.23 (0)	2.73	52.08
CH_4	27.20 (0)	2.39	44.31
CH_3^+	19.07 (0)	2.38	44.51
H_2	6.13 (0)	2.07	31.32

[a] All data were calculated using scaled (by 0.93) MP2(full)/6-31G** vibrational frequencies. [b] Includes vibrational, rotational, and translational contributions, where $RT/2$ was assigned to each rotational and translational degree of freedom. [c] In parentheses is given the number of imaginary frequencies.

Energies and Geometries

Previous theoretical investigations on the $C_2H_7^+$ cation concentrated on the C–C and C–H protonated structures **1** and **2** (Figure 2), presumed to be the two species observed experimentally. The high-level *ab initio* calculations of Raghavachari and co-workers gave a relative energy of 6.8 kcal/mol for the C–H (**2**) vs the C–C protonated species (**1**)[13a] at MP4(SDTQ)/6-31G**//MP2(full)/6-31G*. The authors noted the dramatic differences between the structures optimized at the HF and the correlated level. Similar geometrical changes were reported earlier by Köhler and Lischka, who used the CEPA correlation method.[17]

The present work corroborates but also extends and modifies the previous results. We calculated both **1** (C_2) and **2** (C_s) to be minima. However, the C_s structure **1a**, which is a transition state (at MP2(full)/6-31G**) for rotation of a CH_3 moiety, has essentially the same energy as **1**. At our best level, **1a** is more stable than **1** by 0.3 kcal/mol (Table 2). In the following discussion we will refer only to **1** (the minimum structure), but relative energies at 298 K are based on **1a**. Optimization with polarization functions on hydrogens (MP2(full)/6-31G**) results only in small changes relative to the MP2(full)/6-31G* values (Table 4). At MP2(full)/6-31G**, the C–C distance in the C_2 structure **2** is 1.94 Å and the C–H–C angle is 105.3°. In the C_s structure **2**, which is only a very loose complex at the HF/6-31G* level,[13a] the distances between the hypercoordinated carbon and the three-center bonded hydrogen atoms are 1.215 and 1.193 Å at MP2(full)/6-31G** (Table 4). The relative energies also do not change much on optimization with the fully polarized basis set. At our highest level (Table 2), the C–C protonated structure (**1**) is more stable than the C–H protonated form (**2**) by 6.6 kcal/mol.

However, **2** is not the lowest C–H protonated minimum; the H_2-rotated form **3** is more stable than **2**. The C_s structure **3** is a minimum at HF/6-31G* but not at correlated levels, where the symmetry must be reduced to C_1 to eliminate the imaginary vibrational frequency. At MP2(full)/6-31G**, the C_s structure **3** is the transition state for the interconversion between the two degenerate C_1 forms (**3a**). Nevertheless, the C_s **3** and C_1 **3a** geometries differ very little and are almost indistinguishable energetically. The distances between the hypercoordinated carbon and the hydrogen atoms also involved in the three-center bonding are 1.206 Å in **3** and **3a**. This value is very similar to the equivalent distances in **2**. The differences between the optimized MP2(full)/6-31G** and HF/6-31G* structures in **3** are significant but not as large as those in **2** (Table 4).

The C_1 structure **3a** was found to be more stable than the C_s **2** at all correlated levels. (Table 2 and Figure 4). This emphasizes the importance of including electron correlation in computational potential energy surface analysis. Poirier et al. found a structure similar to **3** to be a saddle point at 3-21G but commented that "this is probably an artifact of the basis set".[18] Moreover, it was not possible to differenciate between **3** and **2**. At our best level, **3** lies 4.4 kcal/mol above the global minimum **1** but is 2.1 kcal/mol more stable than **2**. Hence, the second most stable form of protonated ethane is **3**, with the H_2 attached perpendicular to the C–C bond rather than eclipsed (as in **2**).

Although the point is a minor one, we searched extensively for the transition state between structures **2** and **3**, both of which are minima. Since all the transition-state optimizations either converged to unrelated geometries or did not converge at all, we carried out a series of restrained geometry optimizations with fixed C–C–H_a–H_b dihedral angle (see structures in Table 4). The H–H moiety was rotated step by step from 180° (**2**) to 90° (**3**), and each geometry was optimized at the correlated MP2(full)/6-31G* level. We found a geometry with a dihedral angle of 153° to be the highest in energy, but only 0.14 kcal/mol above **2**. The small energy difference between this geometry and **2** suggests that the transition state interconnecting **2** and **3** must be closely related, structurally and energetically, to both these minima. The energy surface around these stationary points is very flat. All our evidence indicates that the barrier leading from **2** to **3** should be very low. Hence, only the more stable structure **3** should be experimentally accessible.

How easily do the hydrogen atoms exchange? This question is central to the interpretation of the results of Saunders, Cross, et al.[10] Several processes are involved. First, the four nonequivalent hydrogen atoms on the hypercoordinated carbon in **3** exchange by rotation of the CH_4 group around the C–C bond: transition structures **4** and **5** have C_s symmetry and a single negative eigenvalue in the force constant matrix. Their relative energies lie respectively 1.3 and 2.1 kcal/mol above **3** and 5.8 and 6.5 kcal/mol above the global minimum **1**. Second, the C_s structure **6** is the transition state for interconversion of the two minima, **1** and **2**. The geometry of **6** is rather similar to that of **2**. Our best result indicates that the energy of **6** is 7.2 kcal/mol higher than that of **1** and 2.7 kcal/mol above **3**. Third, the rotation of the methyl groups in **1**, via the C_s structure **1a** as transition state, occurs with a barrier of only 0.3 kcal/mol (Table 2). Hence, the energies of all transition states, those interconnecting the minima as well as those for hydrogen exchange, lie *lower* than the dissociation energy into $C_2H_5^+$ and H_2. We calculate the latter to be 10.7 kcal/mol relative to the global minimum **1**. These results agree with Kebarle's experimental dissociation energies of 10.5 ± 2[7c] and 13 kcal/mol[8] and also are consistent with the qualitative observations of Saunders et al.[10]

The D_{3d} structure **7**, with a linear C–H–C bond, is a minimum at HF/6-31G* but not at correlated levels. Its relative energy is 3.2 kcal/mol above **1**. Since the H-bridged (C_{2v}, **8**) ethyl cation is the only $C_2H_5^+$ minimum at correlated levels (the classical form **9** is a minimum at, e.g., HF/6-31G* but not at MP2/6-31G*),[13a] we also tried a set of $C_2H_5^+$·H_2 complexes in C_{2v} symmetry (Figure 3). Structures **10** and **11** (which have exactly the same energy) are both minima at MP2(full)/6-31G**, but they are very loose complexes (Table 5). At that level, the dissociation energies of **10** and **11** into $C_2H_5^+$ (**8**) + H_2 at 0 K are very small (<0.1 kcal/mol). **12** is a transition state for motion of the H_2 moiety parallel to the C–C bond, whereas **13** is a higher order stationary point. Their energies are also given in Table 5. Another possibility for complexation of H_2 to $C_2H_5^+$ is in a less symmetrical C_s form. Structures **14** and **15** (Figure 3) were located as stationary points; however, only **14** is a minimum. **15** is the transition structure for rotation of the H_2 moiety. Starting from the C_s structures **14** and **15**, we tried to find transition states for the addition of H_2 to the ethyl cation. Optimizations in C_s symmetry led to structures **16** and **17** (Figure 3). However, only

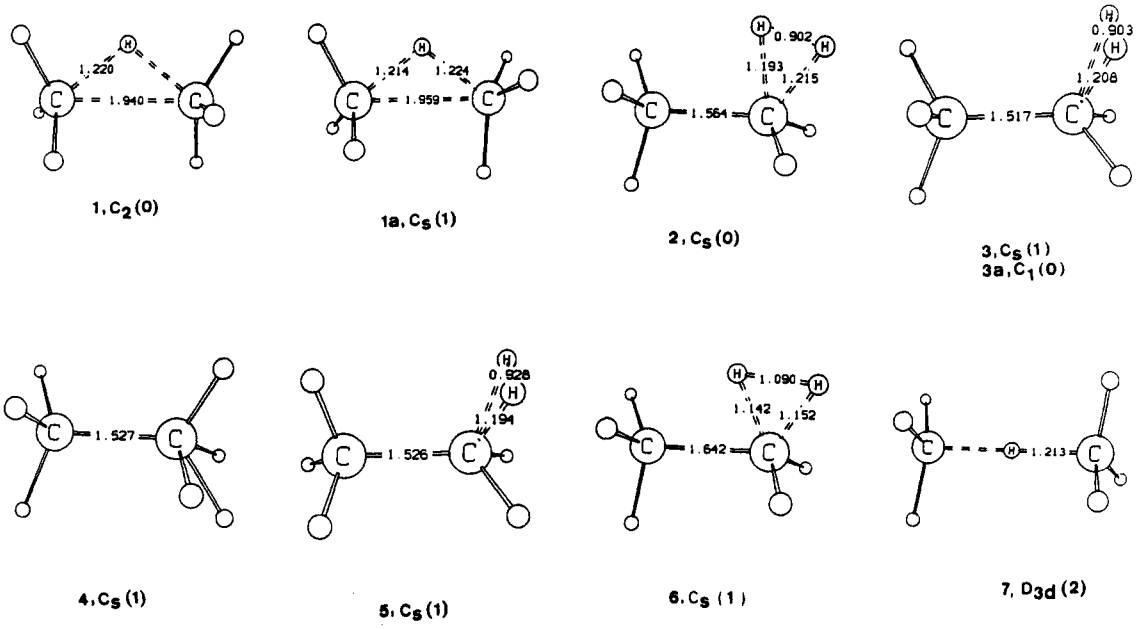

Figure 2. MP2(full)/6-31G** geometries of $C_2H_7^+$ isomers. The number of imaginary frequencies is given in parentheses.

16 is a true transition state; **17** has two negative values in the force constant matrix. At our highest level, **16** lies 2.9 kcal/mol above the ethyl cation **8** and H_2 (Table 5). **17** has essentially the same energy as **16**. We also tried structures where the H_2 approaches the ethyl cation from above. Nevertheless, no minimum or transition state was found. All optimizations in C_s symmetry converged to structures which have two or more imaginary frequencies. The low dissociation energies of the complex-like minima **10**, **11**, and **14** indicate that the H_2 acts as a solvation species around the ethyl cation. These complexes are not expected to be observed experimentally, since the entropic contribution to the energy at any measurable temperature should exceed the small binding energy.

Figure 4 shows the dependence of the relative energies of the bonded species vs theoretical level, with the H-bridged structure **1** taken as the reference. Also included in Figure 4 are values for $CH_4 + CH_3^+$ and $H_2 + C_2H_5^+$. While the relative energies of $CH_4 + CH_3^+$ and of $C_2H_5^+ + H_2$ vary widely, those of the five structures **2–6** remain clustered together. Inclusion of electron correlation at, e.g., MP2(full)/6-31G*, has the largest effect, which is drastic on the relative energy of CH_3^+ and CH_4.

Vibrational Frequencies

Recently, we compared experimental and theoretical vibrational spectra to establish the H-bridged structures of the *sec*-butyl[25] and cyclooctyl cations.[26] The experimental vibrational spectra of $C_2H_7^+$ ions, reported by Lee et al.,[11] invite comparisons with our computed data. Table 6 gives the calculated vibrational frequencies for the three minima **1**, **2**, and **3a** as well as for the methonium cation CH_5^+ in the equilibrium C_s geometry. The experimental data of Lee et al.[11] also are given in this table.

As shown in Table 6a, the three vibrational frequencies assigned by Lee et al. to the C–C protonated species **1** are reproduced nicely by our calculations. The differences between the experimental and the scaled theoretical frequencies are only about 10 cm^{-1} for the three peaks. Of great interest are the vibrations computed at 2042 and 1976 cm^{-1}. As has been shown earlier, IR peaks in this region of the spectrum are characteristic of C–H vibrations in symmetrically 1,2-H-bridged[25] and in transannularly bridged[26] structures. In the present case, the frequency at 2042 cm^{-1} is assigned to the motion of the bridging H parallel to the C–C axis and that at 1976 cm^{-1} to the bridging H moving away from the C–C axis. The large calculated intensities indicate that these vibrations should be prominent in the IR spectrum of the $C_2H_7^+$ ion. Unfortunately, the laser employed by Lee et al. did not permit study below 2400 cm^{-1}.

While the calculated and experimental spectra agree very well for the bridged structure **1**, the same is *not* true for the C–H protonated cation (either **2** or **3**). First, we did not compute any vibration above 3100 cm^{-1} for either **2** or **3**, whereas Lee et al. observed a peak at 3964 cm^{-1} and assigned it to the H–H stretching in a loose $C_2H_5^+ \cdot H_2$ complex.[11] Second, also in contrast to the results of Lee et al., our highest frequencies in **2** and **3** (see Table 6b and c) are not due to H–H stretching but are due to an asymmetric C–H stretch in the CH_3 moiety. The characteristic frequencies associated with the hydrogens in the three-center bond appear more than 1000 cm^{-1} below that claimed by Lee et al. The vibrational frequencies at 2770 cm^{-1} for **2** and 2716 cm^{-1} for **3** are due mainly to H–H stretching. The asymmetrical C–H stretching motions in these three-center bonds give rise to the frequencies at 2229 cm^{-1} for **2** and at 2217 cm^{-1} for **3** (Tables 6b and c).

To check these results at different theoretical levels, we also calculated the vibrational frequencies for **1** and **3** with a double-ζ plus polarization basis set and the CISD electron correlation method (Table 6a and c). The results strongly support our conclusions and also the unpublished frequency calculations of Dupuis, mentioned by Lee et al.[11] While disagreeing with the experimental assignment, our results appear to be much more plausible when they are compared with those of other H_2 complexes, e.g., the computed spectra of the CH_5^+ ion. As shown in Table 6d, the vibrational spectrum of CH_5^+ correlates well with those of **2** and **3**. In the C_s form of the CH_5^+ ion, the H–H stretching vibration is found at 2619 cm^{-1}, while a C–H stretching mode appears at 2382 cm^{-1}. Schreiner et al. have analyzed the vibrational spectrum of the CH_5^+ cation recently.[13c,27] They also conclude that the H–H stretching vibration in the three-center bonds lies below 3000 cm^{-1} (the scaled frequencies are 2633 cm^{-1} for the C_s (**1**) species).

The geometrical parameters given in Table 4 (as well as the energy data) indicate that in **2** and **3** the H_2 moiety is rather tightly bound to the $C_2H_5^+$ cation, that is, a true $C_2H_7^+$ species

(25) Buzek, P.; Schleyer, P. v. R.; Sieber, S.; Koch, W.; Carneiro, J. W. de M.; Vancik, H.; Sunko, D. E. *J. Chem. Soc., Chem. Commun.* **1991**, 671–674.

(26) Buzek, P.; Schleyer, P. v. R.; Vancik, H.; Sunko, D. E. *J. Chem. Soc., Chem. Commun.* **1991**, 1538–1540.

(27) Also see: Komornicki, A.; Dixon, D. A. *J. Chem. Phys.* **1987**, *103*, 5625–5634.

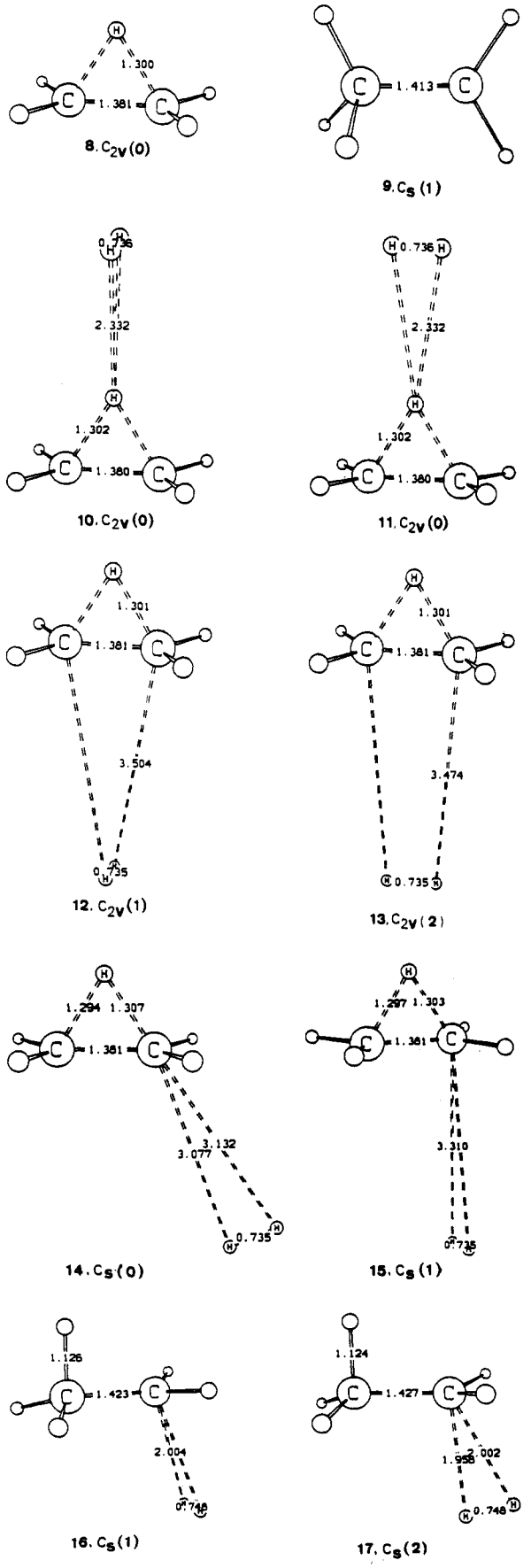

Figure 3. MP2(full)/6-31G** geometries of ethyl cation isomers and $C_2H_5^+ \cdot H_2$ complex-like structures. The number of imaginary frequencies is given in parentheses.

is involved and not just a loose $C_2H_5^+ \cdot H_2$ complex. At all correlated levels, the C–H bond lengths in the three-center bonds are about 1.2 Å, whereas the H–H distances are about 0.9 Å.

Table 4. Selected Geometrical Parameters for $C_2H_7^+$ and CH_5^+ [a]

		HF/ 6-31G*	MP2 (full)/ 6-31G*	MP2 (full)/ 6-31G**
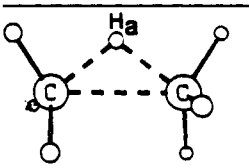	C–C	2.163	1.953	1.940
	$C–H_a$	1.239	1.225	1.220
	∠C–H–C	121.56	105.67	105.29
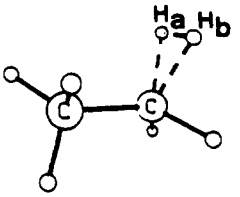	C–C	1.519	1.518	1.517
	$C–H_a$	1.289	1.216	1.205
	$C–H_b$	1.289	1.217	1.206
	$H_a–H_b$	0.814	0.896	0.906
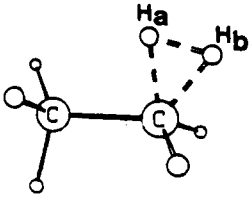	C–C	1.434	1.565	1.564
	$C–H_a$	2.676	1.199	1.193
	$C–H_b$	2.734	1.222	1.215
	$H_a–H_b$	0.733	0.901	0.902
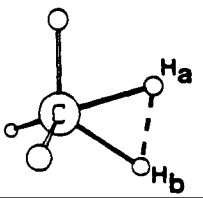	$C–H_a$	1.230	1.185	1.177
	$C–H_b$	1.229	1.182	1.177
	$H_a–H_b$	0.853	0.950	0.957

[a] Distances in angstroms; angles in degrees.

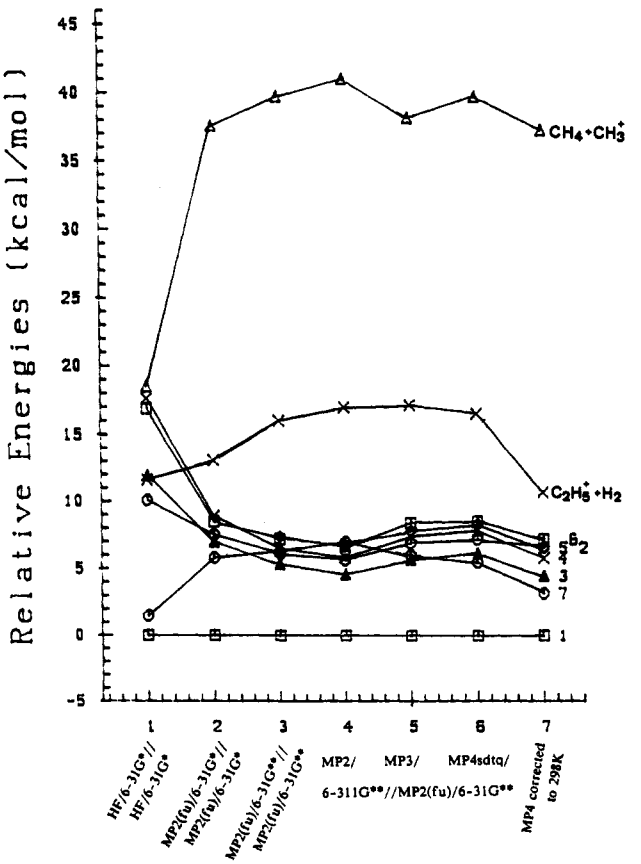

Figure 4. Relative energies of $C_2H_7^+$ isomers as a function of the theoretical level.

Consistent with the shift of the H–H stretching vibration to lower frequencies, the three-center C–H distances in the CH_5^+ ion are smaller and the H–H distance is greater than those in $C_2H_7^+$.

Table 5. Energies of the Complex-like Structures **10**–**17** Relative to $C_2H_5^+ + H_2$[a]

species	MP2(full)/6-31G**// MP2(full)/6-31G**	MP2(full)/6-31G**// MP2(full)/6-31G** + ZPE
10, C_{2v}	−0.94 (0)	−0.05
11, C_{2v}	−0.95 (0)	−0.08
12, C_{2v}	−0.39 (1)	−0.04
13, C_{2v}	−0.35 (2)	−0.09
14, C_s	−0.51 (0)	0.07
15, C_s	−0.42 (1)	−0.02
16, C_s	3.95 (1)	2.92[b]
17, C_s	4.09 (2)	5.90

[a] Energies are in kcal/mol. In parentheses is given the number of imaginary frequencies at MP2(full)/6-31G**. [b] MP4sdtq/6-311G**//MP2(full)/6-31G** corrected to 298 K.

Our results on CH_5^+ agree with the earlier findings.[13c,27] Based on the experimental bonding energy of $C_2H_7^+$ (4 kcal/mol relative to $C_2H_5^+ + H_2$),[8] Lee et al. claimed that their 3964-cm^{-1} frequency agrees with observations for other AH_2 complexes (e.g., H_5^+ and H_7^+).[11] We calculate an energy of 6.2 kcal/mol (at 298 K) for the decomposition of $C_2H_7^+$ (**3**) into $C_2H_5^+$ (**8**) and H_2 (see Table 7 and Discussion below). However, since **2** and **3** are best considered as H_2 complexes of a *classical* ethyl cation (**9**), comparisons of bonding energy should be made on this basis. A "classical" $CH_3CH_2^+$ rotation transition structure can be computed if C_s symmetry and a 0° H–C–C–H dihedral angle are imposed. At MP2(full)/6-31G**, the bridged structure **8** is more stable than the classical **9** by 6.7 kcal/mol (at 0 K). Thus, the actual bonding energy of $C_2H_7^+$ (**3**) should be about 13 kcal/mol. As a consequence, the H–H stretching vibration occurs at much lower frequency than in free H_2. We conclude that the experimental vibrational spectrum[11] of the second $C_2H_7^+$ species does not correspond to that of **3** (or **2**). In addition, the complex-like structures **10**, **11**, and **14** (Figure 3) are too weakly bonded to be responsible for the second $C_2H_7^+$ species detected experimentally.

Discussion

Hiraoka and Kebarle[8] and Poirier et al.[18] summarized their $C_2H_7^+$ results in an energy diagram. Our revised version (Figure 1) contains the same information but is based on newer literature energies for reference compounds (Table 8). Some discrepancies between our theoretical results and those derived from the high-pressure mass spectrometry experiments[8] are evident. Our 4.4 kcal/mol (corrected to 298 K) energy difference between the two stable minima is less than the 7.8 kcal/mol deduced from experiment.[8] Likewise, the calculated 2.7 kcal/mol barrier for rearrangement from **3** to **1**, assumed to proceed via structure **6**, is lower than the experimental value of 5.2 kcal/mol.[8] Also contrary to Kebarle, we computed a barrier of 2.9 kcal/mol (Table 5) for the addition of H_2 to the ethyl cation leading to **3** (see below).

Table 7 summarizes the thermochemical data for eq 3. Our energy for this process diverges by about 2.4 kcal/mol from the value Kebarle reported but is in excellent agreement with more recent data.[28,29] The value of 219 kcal/mol assumed by Kebarle for the heat of formation of the ethyl cation has been revised more recently to 216 kcal/mol.[28-32] (see Table 8). Also given in Table 7 are thermochemical data for the dissociations of $C_2H_7^+$ and CH_5^+ into $C_2H_5^+ + H_2$ and $CH_3^+ + H_2$, respectively (eqs 4 and 5).

$$CH_4 + CH_3^+ \rightarrow C_2H_5^+ (8) + H_2 \quad (3)$$

$$C_2H_7^+ (1) \rightarrow C_2H_5^+ (8) + H_2 \quad (4a)$$

$$C_2H_7^+ (3) \rightarrow C_2H_5^+ (8) + H_2 \quad (4b)$$

$$CH_5^+ \rightarrow CH_3^+ + H_2 \quad (5)$$

For the dissociation of $C_2H_7^+$ (**1**) into $C_2H_5^+$ (**8**) + H_2 (eq 4a), our theoretical enthalpy and Kebarle's directly measured experimental value differ hardly at all (about 1.0 kcal/mol). However, for reaction 4b, the theoretical enthalpy is 2.2 kcal/mol greater than the experimental value (Table 7). The experimental reactions enthalpies and entropies were derived from van't Hoff plots of the measured equilibria. We have not found any consistent difference between experiment and our theoretical results. Note that, for reaction 4b, whereas ΔH and ΔS do not agree at all, the experimental (−1.8 kcal/mol) and the theoretical (−1.2 kcal/mol) free energies (at 298 K) are in reasonable agreement. The dissociation of CH_5^+ is calculated to involve an enthalpy change of 38.9 kcal/mol at 298 K. Nevertheless, in recent high-level calculations on CH_5^+, Schleyer and Carneiro[13b] found the dissociation energy of CH_5^+ to be 42.0 kcal/mol. Kebarle reports a value of 40 kcal/mol for this process; however, more recent experimental data[29,33] lead to an upward revision to 42.5 kcal/mol at 298 K (Table 7). Pople and Curtiss's theoretical heats of formation of small cations agree on average within 2 kcal/mol of the experimental values,[34] but for CH_5^+ the authors calculated a heat of formation (at 298 K) 5.5 kcal/mol greater than the experimental value. Pople's data yield a value of 38.6 kcal/mol (at 298 K) for the dissociation energy of CH_5^+. Our result is closer to that deduced from the more recent experimental determinations.

We have also searched for the elimination pathways of H_2 and CH_3^+ from $C_2H_7^+$ (as well as the pathways for the corresponding reverse reactions for addition). Together with the isomerizations of the $C_2H_7^+$ system discussed above, these processes characterize reaction 1 mechanistically.

We have not carried out dynamics calculations but have explored two possible pathways for the CH_3^+ addition to CH_4 (Figure 5). The first one involves a C_{3v} symmetric approach, in which a hydrogen atom of the CH_4 interacts as donor with the vacant p-orbital of the CH_3^+ cation (Figure 5a). However, no local minimum in C_{3v} was found and, as described below, distortion from C–H–C linearity leads to the C_2 symmetry structure **1**. The second pathway in C_s symmetry involves a side-on interaction of the methyl cation p-orbital with a C–H bond of methane (Figure 5b). When this approach was tested computationally, also by starting the optimization with a reasonably large separation, only structure **1** resulted. At large and fixed C–C distances (>2.43 Å), the most stable $C_2H_7^+$ form is one with a linear C–H–C geometry (cf. Figure 5a). When the carbon atoms are allowed to approach each other, this structure begins to distort and the optimization converges to structure **1** with the central hydrogen atom placed symmetrically between both carbons. These results indicate that the addition of CH_4 to CH_3^+ leads directly to the more stable C_2 structure **1**.

In their cross-beam electron accelerator experiments, Saunders et al.[10] started with deuterium-labeled methane or methyl cation (reactions 6a and 6b). The distribution of isotopically labeled product ions was investigated as a function of collision energy. Extensive hydrogen–deuterium scrambling occurred at low collision energies. However, as the collision energy increased, the deuterium distribution (see eqs 6a and 6b) became nonrandom. $C_2H_2D_3^+$ predominanted in eq 6a and $C_2H_3D_2^+$ in eq 6b.

(28) Lias, S. G.; Liebman, J. F.; Levin, R. D. *J. Phys. Chem. Ref. Data* **1984**, *13*, 695–808.
(29) Traeger, J. C.; McLoughlin, R. G. *J. Am. Chem. Soc.* **1981**, *103*, 3647–3652.
(30) Baer, T. *J. Am. Chem. Soc.* **1980**, *102*, 2482–2483.
(31) Bohme, D. K.; Mackay, G. I. *J. Am. Chem. Soc.* **1981**, *103*, 2173–2175.
(32) Rosenstock, H. M.; Buff, R.; Ferreira, M. A. A.; Lias, S. G.; Parr, A. C.; Stockbauer, R. L. *J. Am. Chem. Soc.* **1982**, *104*, 2337–2345.
(33) Bohme, D. K.; Mackay, G. I.; Schiff, H. I. *J. Chem. Phys.* **1980**, *73*, 4976–4986.
(34) Pople, J. A.; Curtiss, L. A. *J. Phys. Chem.* **1987**, *91*, 155–162.

Table 6. Theoretical Vibrational Frequencies for **1**, **2**, **3**, and the CH_5^+ Ion[a]

(a) Compound **1**

scaled frequency[b]	intensity	scaled frequency[c]	intensity	exptl[11]	approximate normal mode description
3139	45.83	3125	19.37		asym CH stretch of CH_3, asym CH_3s
3136	12.55	3127	7.73	3128	asym CH stretch of CH_3, sym CH_3s
3078	44.47	3083	23.23		asym CH stretch of CH_3, sym CH_3s
3075	12.50	3074	16.09	3082	asym CH stretch of CH_3, asym CH_3s
2936	30.77	2939	15.85	2945	sym CH stretch of CH_3, asym CH_3s
2935	1.77	2990	0.39		sym CH stretch of CH_3, sym CH_3s
2042	49.88	2117	251.35		asym CH stretch of bridging proton
1976	43.68	1933	18.71		sym CH stretch of bridging proton
1410	2.55	1424	0.66		asym ∠HCH bend of CH_3, asym CH_3s
1408	3.09	1425	1.05		asym ∠HCH bend of CH_3, sym CH_3s
1393	30.32	1412	26.08		asym ∠HCH bend of CH_3, sym CH_3s
1387	40.18	1407	31.77		asym ∠HCH bend of CH_3, asym CH_3s
1316	0.27	1313	0.43		sym ∠HCH bend of CH_3 (umbrella mode), sym CH_3
1246	5.40	1248	31.57		sym ∠HCH bend of CH_3 (umbrella mode), asym CH_3
1097	14.79	1109	10.23		asym CH_3 out-of-plane rock – proton out-of-plane distortion
1071	0.24	1086	0.06		CH_3 out-of-plane rock, sym CH_3s
991	62.36	998	131.25		CH_3 in-plane rock, asym CH_3s
815	3.32	817	2.14		CH_3 in-plane rock, sym CH_3s
343	4.78	331	4.02		CC stretch (– sym CH stretch of bridging H)
263	6.37	190	3.95		asym CH_3 out-of-plane rock + proton out-of-plane distortion
236	2.01	213	0.85		CC bond twist

(b) Compound **2**

scaled frequency[b]	intensity	approximate normal mode description
3085	39.29	asym CH stretch of CH_2 + asym CH stretch of CH_3
3067	0.02	asym CH stretch of CH_3
3059	10.61	asym CH stretch of CH_3
2991	30.63	sym CH stretch of CH_2
2951	1.56	sym CH stretch of CH_3 (breathing mode)
2770	17.49	HH stretch of H_2 in the three-center bond
2229	34.72	asym CH stretch of CH in the three-center bond
1536	10.67	bend of CH_2 – ∠HCH bend in the three-center bond (umbrella)
1443	13.47	sym ∠HCH bend of CH_3
1442	9.53	asym ∠HCH bend of CH_3 + asym ∠HCH bend of CH_2
1417	3.79	sym ∠HCH bend of CH_2
1371	29.35	asym ∠HCH bend in CH_2 – asym ∠HCH bend of CH_3
1369	1.26	sym ∠HCH bend of CH_3 (umbrella mode)
1165	0.69	asym ∠HCH bend in CH_3 – asym ∠HCH bend in CH_2
1119	11.04	CH_3 in-plane rock + CH_2·H_2 in-plane rock
935	71.23	CH_3 in-plane rock – CH_2·H_2 in-plane rock + CC stretch
869	5.29	CH_3 out-of-plane rock + CH_2·H_2 out-of-plane rock
780	33.23	CC stretch + CH_2·H_2 in-plane rock
625	126.37	CH_3 in-plane rock – H_2 in-plane rock
289	12.90	CC bond twist + CH_2 twist + H_2C twist
221	23.52	H_2 twist

(c) Compound **3**

scaled frequency[b]	intensity	scaled frequency[c]	intensity	exptl	approximate normal mode description
3061	1.73	3041	0.00	2762	asym CH stretch in CH_3
3051	4.88	3030	1.03	2683	asym CH stretch in CH_3
2967	55.89	2975	41.61	2825	asym CH stretch in CH_2
2952	0.76	2961	0.60	2521	sym CH stretch of CH_3 (CH_3 breathing mode)
2929	46.18	2981	31.24	2601	sym CH stretch of CH_2 – HH stretch of H_2·CH_2
2716	28.42	2832	16.89	3964	HH stretch of H_2·CH_2 + sym CH stretch of CH_2
2217	54.68	2094	60.74		asym CH stretch of H_2·C in three-center bond
1520	0.88	1514	0.55		∠HCH bend of CH_2 – sym CH stretch of H_2·C
1444	13.81	1461	7.42		asym ∠HCH bend of CH_3
1441	16.24	1458	12.96		asym ∠HCH bend of CH_3
1391	3.92	1408	4.44		sym ∠HCH bend of CH_3 (umbrella) + sym ∠H–C–H_2 bend (umbrella)
1328	5.03	1340	6.25		sym ∠HCH bend of CH_3 (umbrella) – sym ∠H–C–H_2 bend (umbrella)
1282	18.46	1210	18.14		asym ∠HCH bend in CH_3 + asym ∠HCH bend in CH_2
1198	32.38	1318	18.41		CH_2 twist – H_2·C rock in H_2·CH_2
1105	5.86	1133	3.87		CH_3 out-of-plane rock + CH_2·H_2 out-of-plane rock
1013	23.11	1047	18.31		CH_3 in-plane rock + CC stretch
908	21.45	927	17.25		CC stretch – CH_3 in-plane rock
740	22.01	760	16.77		CH_3 out-of-plane rock – CH_2·H_2 out-of-plane rock
677	72.15	686	48.44		CH_3 in-plane rock – CH_2·H_2 in-plane rock
259	0.41	282	0.95		CC bond twist + CH_2 twist + H_2·C twist
66	70.14	172	44.47		CC bond twist – H_2·C twist + CH_2 rock

(d) CH_5^+ Ion

scaled frequency[b]	intensity	approximate normal mode description
3107	85.60	asym CH stretch of CH_3
3015	79.77	asym CH stretch of CH_3
2892	101.97	sym CH stretch of CH_3 (breathing mode) + CH stretch of CH_2

Table 6 (Continued)

(d) CH_5^+ Ion

scaled frequency[b]	intensity	approximate normal mode description
2619	36.44	sym CH stretch of CH_2 + H_2 stretch + CH stretch of CH_3 (breathing mode)
2382	64.14	asym CH stretch of CH_2
1507	6.35	∠HCH bend of CH_2 – sym ∠HCH bend of CH_3 (umbrella)
1422	0.03	asym ∠HCH bend of CH_3
1403	0.92	sym ∠HCH bend of CH_3
1258	58.15	CH_3 out-of-plane rock + H_2 out-of-plane rock
1228	34.24	sym ∠HCH bend of CH_3 (umbrella)
710	243.52	CH_3 in-plane rock – H_2 stretch
305	49.14	H_2 twist

[a] Vibrational frequencies are in cm^{-1}; intensities are in km/mol. [b] Frequencies calculated at the MP2(full)/6-31G** level, scaled by 0.93. [c] Frequencies calculated at the DZ+P/CISD level, scaled using out-of-plane and bending mode internal coordinate scaling factors.

$$CD_3^+ + CH_4 \rightarrow C_2H_2D_3^+ + H_2$$
$$C_2H_3D_2^+ + HD$$
$$C_2H_4D^+ + D_2 \qquad (6a)$$

$$CH_3^+ + CD_4 \rightarrow C_2HD_4^+ + H_2$$
$$C_2H_2D_3^+ + HD$$
$$C_2H_3D_2^+ + D_2 \qquad (6b)$$

These results were interpreted in terms of $C_2H_nD_{7-n}^+$ (n = 2, 3, 4) intermediates. At low collision energies, the rate of hydrogen–deuterium scrambling is fast relative to the rate of decomposition. As a consequence, a statistical distribution of isotopically labeled products results. As the relative collision energy increases, however, there is less time for total scrambling. This leads to a nonrandom isotopic distribution in the final products. This nonrandom product distribution found at higher energy led Saunders et al. to assume that the intermediate species has a structure like **3** (or **2**), with the extra proton associated with only a single carbon atom. They argued that the symmetrical structure **1** would lead (via reaction 6a) to equimolar formation of $C_2H_3D_2^+$ and $C_2H_2D_3^+$ (if bridging hydrogen participates in the dissociation) or to $C_2H_4D^+$ and $C_2H_2D_3^+$ (if bridging hydrogen did not participate in the dissociation). Similar behavior should be expected for reaction 6b (in which the Hs and Ds in the initial reactants are interchanged).[10]

Our calculational results indicate that **1** (rather than **2** or **3**) is the first species formed from the methyl cation and methane. The rearrangement from **1** into **3** involves transition state **6** (7.2 kcal/mol above **1**), leading, via **2** (6.6 kcal/mol above **1**), to **3**. The rotation of the CH_4 group around the C–C bond in **3** renders all the hydrogens bonded to the hypervalent carbon equivalent. The barrier is 1.3 kcal/mol (transition structure **4**). Although **2**, as well as **3**, already has partial H–H bonding (one of the Hs comes from the bridging position, see structure **6**), the interchange between the hydrogens in the hypervalent carbon involves a lower barrier (1.3 kcal/mol) than the return to **1** (2.7 kcal/mol). The low vibrational frequency calculated for the H–H stretching in the three-center bonds also indicates the H–H bonding to be only partial. If the hydrogens bonded to the hypervalent carbon interchange, any pair of them can be lost to form the $C_2H_5^+$ ion.

If, as the calculations indicate, partial scrambling in the CH_4 moiety is easier than the total scrambling, it is possible to reconcile Saunders's experimental results with the initial formation of **1**. Consider the isotopic labeled reactions 6a and 6b. For reaction 6a, after rearrangement of **1** into **3**, we will have an equal amount of CD_3-CH_4^+ and of CH_3-CHD_3^+. Assuming all the Hs in CD_3-CH_4^+ to be equivalent, decomposition into ethyl cation and H_2 would give $C_2H_2D_3^+$ as the only product. On the other side, decomposition of CH_3-CHD_3^+ leads to both $C_2H_3D_2^+$ and $C_2H_4D^+$. This means that statistically we will observe a predominance of $C_2H_2D_3^+$ over $C_2H_3D_2^+$ (as well as over $C_2H_4D^+$) by a factor of 2 (assuming no isotope effect). This agrees with the experiment of Saunders et al.[10] The same interpretation can be applied to reaction 6b if the Hs and Ds are interchanged. In this case the main product is $C_2H_3D_2^+$.

Table 7. Thermochemical Data for Reactions 3–5[a]

	theor[b]		exptl[c]	
reaction	ΔH	ΔS	ΔH	ΔS
$CH_4 + CH_3^+ =$ $C_2H_5^+$ (**8**) + H_2	−26.6	−2.9	−24.2 −27.3[d]	
$C_2H_7^+$ (**1**) = $C_2H_5^+$ (**8**) + H_2	10.7 11.4[e]	25.2	11.8 ± 0.4	25 ± 1
$C_2H_7^+$ (**3**) = $C_2H_5^+$ (**8**) + H_2	6.2 7.3[e]	26.7	4.0 ± 0.5	19.6 ● 1.5
$CH_5^+ = CH_3^+ + H_2$	38.9 42.0[e] 38.6[g]	23.8	40.0 42.5[f]	

[a] All data are at 298 K; ΔH in kcal/mol; ΔS in eu. [b] This work. MP4(sdtq)/6-311G**//MP2(full)/6-31G** corrected to 298 K. [c] Reference 8. [d] ΔH_f of $C_2H_5^+$ = 216 kcal/mol; ΔH_f of CH_3^+ = 261.3 kcal/mol (ref 29); ΔH_f of CH_4 = −18 kcal/mol (ref 28). [e] At 0 K, ref 15b. [f] ΔH_f of CH_5^+ = 218.8 kcal/mol (ref 33); ΔH_f of CH_3^+ = 261.3 kcal/mol (ref 29). [g] Reference 34.

We also investigated possible pathways for H_2 elimination from $C_2H_7^+$. It is inherently likely that $C_2H_7^+$ loses H_2 by 1,1-elimination, since **3** has the form of a $C_2H_5^+$·H_2 complex. Reasoning from the other direction, H_2 would have to attack the bridged form of the $C_2H_5^+$ cation, which is the only minimum at correlated levels.[13a] Since 1,2-H_2 attack in C_{2v} symmetry (via structures **10**–**13**) is forbidden, the most probable pathway would be a less symmetrical attack concerted with movement of the bridging H in $C_2H_5^+$ (**8**). Here we investigate two pathways (Figure 6). In the first, the H_2 approaches the ethyl cation from the backside in C_s symmetry (pathway A in Figure 6). Starting from **15** we could locate the transition state **16**, 2.9 kcal/mol above the bridged ethyl cation **8** and H_2. Starting from the H_2 rotated structure **14**, **17** is found, but it has two negative eigenvalues in the force constant matrix. The energy of **17** is very similar to that of **16** (Table 5). In the second pathway, the H_2 molecule approaches the ethyl cation from above (pathway B in Figure 6). We could locate two stationary points in C_s symmetry, but none of them is a true transition state; they have two or three imaginary frequencies. Moreover, the energies of these high-order stationary points are higher than that of **16**. Thus, in the better mechanism (A), the H_2 molecule approaches the ethyl cation in C_s symmetry, leading to **3**. While H_2 approaches one of the carbons, the bridging hydrogen simultaneously moves to the other carbon. This process involves a barrier of 2.9 kcal/mol. The corresponding barrier for dissociation of $C_2H_7^+$ (**3**) into $C_2H_5^+$ (**8**) + H_2 is 9.1 kcal/mol (Table 2).

Continuing interest in gas-phase proton-transfer reactions has led to the definition of two related quantities, proton affinity and gas-phase basicity.[35] The proton affinity gives a quantitative

(35) Dixon, D. A.; Lias, S. G. In *Molecular Structure and Energetics*; Liebmann, J. F., Greenberg, A., Eds.; VCH Publishers, Inc.: Weinheim, Germany, 1987; Vol. 2, Chapter 7.

Table 8. Experimental and Theoretical Heats of Formation of Cationic Species (in kcal/mol at 298 K)

researchers	year	CH_3^+	$C_2H_5^+$	CH_5^+	$C_2H_7^+$	ref
			Experimental			
Lossing et al.	1970	261	219			41
Franklin et al.	1972			222.1	218.8	42
Kebarle et al.	1976			221.1	215	8
					207.2	8
McCulloh et al.	1976	262.7[a]				43
Rosenstock et al.	1977	262[a]	219			44
Houle et al.	1979	261.8 ± 0.5	219.2 ● 1.1			45
Baer	1980		218.2 ● 1.0[a]			30
			215.3 ± 1.0			30
Bohme et al.	1980			218.8 ± 2.1		33
Bohme et al.	1981		216.6 ± 1.7		204.8	31
Traeger et al.	1981	261.3 ± 0.4	216.0 ± 0.5			29
Rosenstock et al.	1982		215.9			32
Lias et al.	1984		215.6	216.0	202.0	28
				217.5		28
Anicich et al.	1984	260.5				46
			Theoretical			
Moran et al.	1985	260.4				47
Pople et al.	1987	261.6		223.0		34

[a] ΔH_f at 0 K.

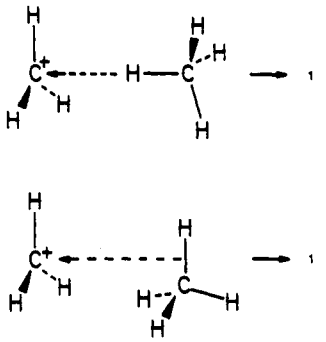

Figure 5. Two possible pathways for addition of CH_4 to CH_3^+. (a, top) The CH_3^+ attacks CH_4 "end-on", initially along a C_{3v} symmetry pathway. A hydrogen atom of CH_4 acts as a σ-donor to the vacant p-orbital of the methyl cation. (b, bottom) CH_3^+ attacks "side-on" with a C–H bond of CH_4 acting as a σ-donor. Both pathways lead to the C_2 symmetry structure **2**.

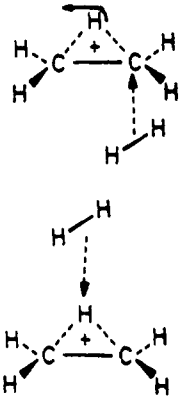

Figure 6. Two possible pathways for addition of H_2 to the ethyl cation. (a, top) The H_2 adds to $C_2H_5^+$ at the backside. (b, bottom) H_2 attacks $C_2H_5^+$ from above. Both mechanisms are concerted. While H_2 attacks one of the carbons, the bridging H moves to the other. This leads to the C_s structure **3**.

measure of the intrinsic basicity of a chemical compound[33,36] and is defined as the negative of the standard enthalpy change of the reaction between a base and a proton to give an acidic species.[35,37] For methane and ethane, the reactions defining the proton affinities are given in eqs 7a and 7b.[32] Combining these equations gives the relative proton affinity of ethane versus methane (eq 8).

$$CH_4 + H^+ \rightarrow CH_5^+ \quad (7a)$$

$$C_2H_6 + H^+ \rightarrow C_2H_7^+ \quad (7b)$$

$$CH_4 + C_2H_7^+ \rightarrow CH_5^+ + C_2H_6 \quad (8)$$

Table 9 summarizes the reported values for proton affinities (PAs) of methane and ethane and the results of the present study. The experimental values diverge considerably, not only due to the operationally different experiments but also due to the use of several standard reference scales. As shown in Table 8, the experimental heats of formation (on which the absolute PA values are based) of the cationic species vary considerably. The most recent determinations[38,39] of the PA of methane give values between 130 and 131.6 kcal/mol (Table 9). For ethane there are two ranges of values, corresponding to the two protonated ethane isomers. The experimental PA of the more stable species was found to be between 137 ± 2[7c] and 146.9[40] kcal/mol; the PAs range from 131[8] to 133 kcal/mol for the other species (Table 9). Although the absolute experimental estimates vary considerably, the PA difference between methane and ethane (to give the more stable $C_2H_7^+$, **1**) as determined in each individual investigation is rather constant, about 12 kcal/mol.[8,28,31,33,40] This agrees with our computed results, corrected to 298 K (also given in Table 9). We calculate a PA of 130.0 kcal/mol for methane; for ethane the two values are 142.5 and 138.1 kcal/mol, leading to the C–C (**1**) and C–H (**3**) protonated ethane forms, respectively. The corresponding differences between the PAs of ethane and of methane, given by the standard enthalpy change of reaction 8, are 12.5 and 8.1 kcal/mol (Table 9). These differences as well as the individual PAs are in good agreement with previous theoretical results.[15b,34]

(36) Aue, D. H.; Bowers, M. T. In *Gas-Phase Ion Chemistry*; Bowers, M. T., Ed.; Academic Press: New York, 1979; Vol. 2.
(37) DeFrees, D. J.; McLean, A. D. *J. Comput. Chem.* **1986**, *7*, 321–333.
(38) Adams, N. G.; Smith, D.; Tichy, M.; Javahery, G.; Twiddy, N. D.; Ferguson, E. E. *J. Chem. Phys.* **1989**, *91*, 4037–4042.
(39) Lias, S. G.; Bartness, J. E.; Liebmann, J. F.; Holmes, J. L.; Levin, R. D.; Mallard, W. G. *J. Phys. Chem. Ref. Data* **1988**, *17*, Suppl. 1.
(40) McMahon, T. B.; Kebarle, P. *J. Am. Chem. Soc.* **1985**, *107*, 2612–2617.
(41) Lossing, F. P.; Semeluk, G. P. *Can. J. Chem.* **1970**, *48*, 955–965.
(42) Chong, S.-L.; Franklin, J. L. *J. Am. Chem. Soc.* **1972**, *94*, 6347–6351.
(43) McCulloh, K. E.; Dibeler, V. H. *J. Chem. Phys.* **1976**, *64*, 4445–4450.
(44) Rosenstock, H. M.; Draxl, K.; Steiner, B. W.; Herron, J. T. *J. Phys. Chem. Ref. Data* **1977**, *6*, Suppl. 1.
(45) Houle, F. A.; Beauchamp, J. L. *J. Am. Chem. Soc.* **1979**, *101*, 4067–4074.
(46) Anicich, V. H.; Blake, G. A.; Kim, J. K.; McEwan, M. J.; Huntress, W. T., Jr. *J. Phys. Chem.* **1984**, *88*, 4608–4617.
(47) Shields, G. C.; Moran, T. F. *J. Phys. Chem.* **1985**, *89*, 4027–4031.

Table 9. Experimental and Theoretical Proton Affinities (PA) of Methane and Ethane (in kcal/mol at 298 K)

researchers	year	$PA(CH_4)$	$PA(C_2H_6)$	$PA(C_2H_6) - PA(CH_4)$	ref
			Experimental		
Franklin et al.	1972		127.1		42
Bohme et al.	1975		140.4		*a*
Kebarle et al.	1975		137.4 ± 2		7c
Kebarle et al.	1976	127	131.8	4.8	8
			139.6	12.6	8
Bohme et al.	1980	130.5 ± 2			33
Bohme et al.	1981		142.1 ± 1.2		31
Kebarle et al.	1982	130	133	3	*b*
			141, 142	11, 12	*b*
Lias et al.	1984	132.0	143.6	11.6	28
Kebarle et al.	1985	134.7	146.9	12.2	40
Lias et al.	1988	131.6			39
Adams et al.	1989	130.0			38
			Theoretical		
Yamabe et al.	1984	127.7	135.6	7.9	15b
			139.7	12.0	15b
Dixon et al.	1987	128.5			30
Pople et al.	1987	128.4			34
Kutzelnigg et al.	1990	130.5			14a
this work		130.0	142.5 (**1**)	12.5 (**1**)	
			138.1 (**3**)	8.1 (**3**)	

[a] Bohme, D. K. In *Interactions between Ions and Molecules*; Ausloos, P., Ed.; Plenum Press: New York, 1975; p 489. [b] Hiraoka, K.; Kebarle, P. *Radiat. Phys. Chem.* **1982**, *20*, 41–49.

Conclusions

Our analysis of the $C_2H_7^+$ potential energy surface reveals three minima, the C–C protonated structure **1** and the C–H protonated forms **2** and **3**. Only **1** and **2** have been considered before, but we find **3** to be 2.1 kcal/mol more stable than **2**. However, **2** and **3** are very similar and have a low conversion barrier for **2** into **3** (0.1 kcal/mol), so that only **1** and **3** should be observable experimentally; **3** is less stable than **1** by 4.4 kcal/mol. The methyl cation addition to methane or the reverse process, loss of CH_3^+ from $C_2H_7^+$, is interpreted in terms of a direct interaction between the methyl carbon and a C–H bond of methane leading to **1**. The latter rearranges into **3** with a barrier of 7.2 kcal/mol. Structure **3** can lose H_2 by 1,1-elimination. While the reaction of methane with the methyl cation does not require an activation energy, the H_2 elimination from $C_2H_7^+$ (**3**) requires a barrier of 9.1 kcal/mol. The reverse addition reaction is calculated to involve a barrier of 2.9 kcal/mol. The barrier for conversion of **1** into **3** (7.2 kcal/mol) is calculated to be lower than the barrier for dissociation into $C_2H_5^+ + H_2$ (13.6 kcal/mol). Hence, under favorable experimental circumstances, it is possible to observe deuterium scrambling when starting with labeled CH_3^+ and CH_4.

The vibrational spectrum of **1** is characterized by the C–H stretching vibrations of the symmetrical bridging proton. As in other H-bridged species, these vibrations occur between 1900 and 2200 cm^{-1}. Other C–H stretching modes computed for **1** agree with those deduced experimentally. Nevertheless, neither **2** nor **3** can explain the second set of experimental spectral data. In particular, the experimental 3964-cm^{-1} H–H stretching mode indicates a relatively weak bond of the H_2 moiety to the $C_2H_5^+$ ion. Complexes between H_2 and bridged $C_2H_5^+$ (**8**) were located, but these are too weakly bound to be candidates for the second $C_2H_7^+$ species detected experimentally.

The proton affinity of methane is calculated to be 130.0 kcal/mol. The two values for ethane are 142.5 kcal/mol, leading to the more stable $C_2H_7^+$ species, and 138.1 kcal/mol, leading to the second species.

Acknowledgment. This work was supported at Erlangen by the Deutsche Forschungsgemeinschaft, the Fonds der Chemischen Industrie, the Volkswagen-Stiftung, and the Convex Computer Corporation; in Georgia by the U.S. Department of Energy; and in Calgary by the Natural Sciences and Engineering Research Council of Canada. J. W. de M. Carneiro thanks CNPq-Brazil for financial support and DAAD-Germany for a grant during his stay in Erlangen.